Article

A Performance Review of Reflectance Based Algorithms for Predicting Phycocyanin Concentrations in Inland Waters

Igor Ogashawara [1,*], **Deepak R. Mishra** [2], **Sachidananda Mishra** [3], **Marcelo P. Curtarelli** [1] **and José L. Stech** [1]

[1] Remote Sensing Division, National Institute for Space Research, Avenida dos Astronautas, 1758, São José dos Campos, SP 12227-010, Brazil; E-Mails: mpedroso@dsr.inpe.br (M.P.C.); stech@dsr.inpe.br (J.L.S.)

[2] Department of Geography, University of Georgia, 210 Field Street, Athens, GA 30602,USA; E-Mail: dmishra@uga.edu

[3] Dow Agrosciences, 9330 Zionsville Road, Indianapolis, IN 46268, USA; E-Mail: sm1287@msstate.edu

* Author to whom correspondence should be addressed; E-Mail: igoroga@gmail.com; Tel.: +55-123-208-6484; Fax: +55-123-208-6488.

Abstract: We evaluated the accuracy and sensitivity of six previously published reflectance based algorithms to retrieve Phycocyanin (PC) concentration in inland waters. We used field radiometric and pigment data obtained from two study sites located in the United States and Brazil. All the algorithms targeted the PC absorption feature observed in the water reflectance spectra between 600 and 625 nm. We evaluated the influence of chlorophyll-*a* (chl-*a*) absorption on the performance of these algorithms in two contrasting environments with very low and very high cyanobacteria content. All algorithms performed well in low to moderate PC concentrations and showed signs of saturation or decreased sensitivity for high PC concentration with a nonlinear trend. MM09 was found to be the most accurate algorithm overall with a RMSE of 15.675%. We also evaluated the use of these algorithms with the simulated spectral bands of two hyperspectral space borne sensors including Hyperion and Compact High-Resolution Imaging Spectrometer (CHRIS) and a hyperspectral air borne sensor, Hyperspectral Infrared Imager (HyspIRI). Results showed that the sensitivity for chl-*a* of PC retrieval algorithms for Hyperion simulated data were less noticable than using the spectral bands of CHRIS; HyspIRI results show that SC00 could be used for this sensor with low chl-*a* influence. This review of reflectance

based algorithms can be used to select the optimal approach in studies involving cyanobacteria monitoring through optical remote sensing techniques.

Keywords: cyanobacteria; phycocyanin; chlorophyll-*a*; band ratio; remote sensing reflectance; hyperspectral sensors

1. Introduction

Cyanobacteria commonly known as blue-green (BG) algae are an important phytoplankton class [1] and have received increasing attention because of their occurrence in inland eutrophic waters around the world [2]. The abundant growth of cyanobacteria in aquatic systems creates problems for water resource managers and policy makers due to their capacity to produce toxins also known as "cyanotoxins", which are a major concern for human health [3,4]. Some of the genera of these BG algae produce toxins which cause hepatotoxic, neurotoxic and dermatotoxic effects and general inhibition of protein synthesis in animals and humans [3]. One of the first cases of human fatalities associated with cyanobacteria and their toxins occurred in 1996 at Caruaru, PE, Brazil, where exposure through renal dialysis led to the death of approximately fifty patients [4]. Besides their toxic characteristic, Cyanobacterial Harmful Algal Blooms (CHABs) also degrade aquatic habitats due to their malodorousness [3,5] and the appearance of a scum layer or thick mat on the surface of water.

Tropical aquatic systems such as Brazilian reservoirs are some of the most suitable places where BG algae can multiply very rapidly. It is because the temperature range (25–35 °C) required to achieve BG algae maximal specific rates of growth matches with the average temperature of these aquatic systems [6]. Several BG algae have confirmed their apparent high carbon affinities since they could maintain slow net growth even at pH > 10 [7]. Light and nutrient availability are also characteristics which promote CHABs [5]. These facts enhance the importance of monitoring BG algae presence in water supply and recreational reservoirs. However, traditional monitoring methods consist of collection of field samples, laboratory analysis, and manual cell counts. These methods are time-consuming, labor intensive and costly [8]. Efficient alternative methods should be developed in order to improve the monitoring of CHABs and remote sensing has been proved as a valuable tool for this application [9].

For remote sensing techniques, phycocyanin (PC) which is a characteristic photosynthetic pigment in inland BG algae, has been used as a proxy due to its distinct optical characteristic (absorption peak at ~620 nm) [5,10–12]. Initially, cyanobacterial biomass was estimated mostly from chlorophyll-*a* (chl-*a*) concentration since it is the primary and dominant photosynthetic pigment in BG algae [13]. However, recent studies have documented that chl-*a* is not an accurate estimator of cyanobacterial biomass since it is common to almost all phytoplankton groups [14]. Therefore, recent studies have evaluated the utility of PC to estimate BG algae abundance, particularly when BG algae are associated with other non-harmful phytoplankton groups [15]. Most of the researchers have been exploiting the PC absorption feature between 615 and 630 nm to develop empirical and semi-analytical models to detect presence of BG algae in water bodies. However, Mishra *et al.* [5] proposed the use of a band at 600 nm since it has less influence of chl-*a* absorption when compared to 620 nm and it also has a significant absorption component by PC.

Thus far, five different algorithms have been proposed for the quantification of BG by exploiting the PC absorption feature: a semi-empirical baseline algorithm (DE93) [16], a single reflectance band ratio algorithm (SC00) [17], a nested semi-empirical band ratio algorithm (SI05) [10], a new single reflectance band ratio algorithm (MI09) [5] and a three band algorithm (HU10) [11]. The baseline algorithm [16] adds reflectance at two wavelengths (600 and 648 nm) to draw a reference baseline, and subtracts the reflectance at 624 nm which is the absorption maximum of PC. The single reflectance ratio [17] uses a PC fluorescence peak of around 650 nm and the PC absorption peak around 625 nm. The nested band ratio [10] algorithm was developed for the Medium Resolution Imaging Spectrometer (MERIS) sensor from the European Space Agency (ESA). To match the MERIS band configuration, it uses 620 nm as the PC absorption maximum and estimates PC concentrations from a semi-analytical inversion procedure using the 620 nm band. The model also addresses the chl-*a* influence at the PC absorption band (620 nm). The new single reflectance ratio [5] uses reflectance at 700 nm as reference, and targets PC absorption at 600 nm in order to minimize the chl-*a* interference. The three band algorithm [11] uses 725 nm as reference and targets the PC absorption by using the difference in the reflectance at 600 nm and 615 nm.

All these algorithms were developed for eutrophic waters involving various study sites worldwide with different optical properties. DE93 used coefficients of inherent optical properties in 10 shallow eutrophic lakes in The Netherlands. SC00 dataset was obtained from a hypereutrophic lake, Carter Lake, in Nebraska, USA. SI05 was developed from datasets from two lakes in The Netherlands: Lake Loosdrecht and Lake Ijsselmeer. MI09 was developed in laboratory using two different laboratory cultured cyanobacterial species. HU10 was developed using data from two shallow eutrophic lakes in the United Kingdom. However, all these algorithms were developed for latitudes higher than 35° and they have not been validated for low latitude areas such as the tropical reservoir in Brazil used in this study. In this research, we have intensively reviewed the performance of the aforementioned algorithms using two unique datasets collected from a tropical reservoir in Brazil and aquaculture ponds in Mississippi, USA. The specific objectives of this research are: (1) to compare and evaluate the performance of the existing reflectance based PC algorithms in two different environmental settings with very high and very low concentrations of chl-*a* and PC, (2) to apply the existing PC algorithms to a synthetic dataset that was simulated using a Gaussian function as the spectral response function of Hyperion, Compact High-Resolution Imaging Spectrometer (CHRIS) and Hyperspectral Infrared Imager (HyspIRI), and (3) to examine the influence of chl-*a* on the performance of these algorithms.

2. Materials and Methods

2.1. Study Sites

We collected field data from two study sites. The first dataset was acquired from the Funil Reservoir located in Itatiaia, RJ, Brazil during 2–5 April 2013, and the second dataset was collected from catfish aquaculture ponds located at the Thad Cochran National Warmwater Aquaculture Center, Stoneville, MS, USA during 13–16 July 2010 and 28–29 April 2011. A summary of study sites, the field campaigns and descriptive statistics of pigments and nutrient concentrations are shown in Table 1.

Funil Reservoir was constructed during the late 1960s by the damming of the Paraíba do Sul River in Southeast Brazil. This hydrographic basin connects three economically important Brazilian states including Minas Gerais, Rio de Janeiro, and São Paulo. It serves as the primary source of drinking water for domestic supply, irrigation, industrial self-supply systems, aquaculture, and hydroelectric power generation [18]. The reservoir receives waste from one of the main Brazilian industrial areas that has enhanced the eutrophication process in recent decades, consequently causing frequent and intense cyanobacterial blooms [19].

The water for all catfish aquacultures in northwest Mississippi comes from wells pumping the Mississippi River Alluvial Aquifer [12]. It is also known that commercial pond culture of channel catfish is practical only in regions with the proper temperature regime—around 25–30°C—for reproduction and rapid growth. According to Tucker [20], the region has the appropriate climatic condition, soil type and water supply for a successful pond culture of channel catfish. However, management practice such as addition of excessive nutrients in the form of commercial catfish food causes phytoplankton blooms dominated by cyanobacteria during warm periods.

The datasets collected from the two study sites represent extreme range of chl-*a* and PC concentrations and are suitable for performance evaluations of the PC algorithms. For example, average PC in Funil Reservoir was found to be 14.52 (µg/L), whereas the catfish pond average PC reading was 241.51 (µg/L) (Table 1). Similar extremes were observed for chl-*a* as well (Table 1). The observed standard deviation among datasets was helpful in reviewing the performance of the above algorithms at very low and very high concentration ranges and also at a varying chl-*a* absorption range.

Table 1. Summary statistics for chl-*a* and phycocyanin (PC) pigment concentrations at study sites.

		Funil Reservoir	Catfish Ponds
Surface Area (km^2)		40	0.004–0.03
Mean depth (m)		20	1.1
Time frame of field campaigns (years)		2013	2010–2011
Total samples		16	23
	Maximum	52.78	831.35
	Minimum	4.92	59.79
Chl-a (µg/L)	**Range**	47.86	771.56
	Average	19.49	230.2
	Standard Deviation	14.79	176.16
	Maximum	35.95	857.08
	Minimum	9.16	68.13
PC (µg/L)	**Range**	26.79	788.95
	Average	14.52	241.51
	Standard Deviation	7.70	215.72
Total Nitrogen (µg/L)	**Maximum**	1,620	8,000 [12]
	Minimum	100	4,000 [12]
Total Phosphorus (µg/L)	**Maximum**	37.77	500 [12]
	Minimum	16.46	800 [12]

2.2. Remote Sensing Reflectance

Field radiometric measurements in the Funil Reservoir, Brazil were acquired during 2–5 April , 2013. Radiance and irradiance measurements were carried out using the RAMSES hyperspectral radiometers (TriOS GmbH, Oldenburg, Germany). Measurements were acquired in the visible and near-infrared range of the spectrum (360–900 nm) with 3.3 nm spectral resolution (0.3 nm accuracy). Six sensors were used, two irradiance and four radiance sensors, acquiring data simultaneously. The two irradiance sensors centered at nominal (excluding effects of wave motion) viewing zenith angle (θ_v) of 90° pointed upward (for downwelling irradiance, E_d) and downward (for upwelling irradiance, E_u) directions. A radiance sensor was also pointed downward to measure the upwelling radiance (L_u). These three measures were collected above and below (below the air-water interface, 1m, 2m and 3m) the water surface. On the top of the boat, a radiometer with an optical fiber and cosine diffuser (yielding a hemispherical field of view, FOV), pointed upward to acquire the incident spectral irradiance (E_s). The other two radiometers with a 7° FOV were also on the top of the boat and were centered at nominal θ_v of 40° in two different directions: upward for the sky radiance (L_s) and downward direction for the radiance received by the sensor pointed at the water surface (L_w).

For the catfish ponds, a dual sensor-system with two inter-calibrated Ocean Optics spectroradiometers (Ocean Optics Inc., Dunedin, FL, USA) were used to acquire remote sensing reflectance (R_{rs}) data in the range 400–900 nm with a sampling interval of 0.3 nm. The first radiometer was equipped with a 25° FOV optical fiber pointed downward to measure the upwelling radiance just below the air-water interface, expressed in digital numbers ($DN_{Lu(\lambda)}$). The second radiometer was equipped with an optical fiber and cosine diffuser (yielding a 180° FOV), pointed upward to acquire above surface downwelling irradiance, also expressed in digital numbers ($DN_{Ed(\lambda)}$). The inter-calibration of the radiometers was accomplished by measuring the upwelling radiance of a white Spectralon reflectance standard (Labsphere, Inc., North Sutton, NH, USA) simultaneously with incident irradiance. The two radiometers were inter-calibrated immediately before and after measurements in each sampling site.

R_{rs} for the optical measures was calculated based on Mobley [21]. For Funil Reservoir, R_{rs} was calculated based on Equation 1 and for catfish ponds based on Equation 2.

$$R_{rs}(\lambda) = \frac{tL_u(\lambda)}{n^2 E_d(\lambda)} F_i(\lambda) \tag{1}$$

where, t is the transmittance at the air-water interface (0.98); n is the refractive index of water (1.34); and $F_i(\lambda)$ is the spectral immersion coefficient [22].

$$R_{rs}(\lambda) = \frac{tDN_{Lu}(\lambda)DN_{Ed,ref}(\lambda)\rho_{ref}(\lambda)}{n^2 DN_{Ed}(\lambda)DN_{Lu,ref}(\lambda)\pi} F_i(\lambda) \tag{2}$$

where, $DN_{Lu,ref}$ and $DN_{Ed,ref}$ are digital numbers representing upwelling radiance and downwelling irradiance over the white Spectralon panel; ρ_{ref} is the irradiance reflectance of the Spectralon panel.

The spectral immersion coefficient for each sensor was derived by following Equation (3) [22].

$$F_i(\lambda) = \frac{n_w(\lambda)(n_w(\lambda) + n_g(\lambda))^2}{(1 - n_g(\lambda))^2} \tag{3}$$

where, n_w is the wavelength-dependent refractive index of freshwater and can be estimated using Equation (4) [23]. n_g is the corresponding index of the glass window of the radiance sensor.

$$n_w(\lambda) = 1.325147 + \frac{6.6096}{\lambda - 137.1924} \tag{4}$$

At both study sites, for each sample point, multiple reflectance measurements were acquired and for which the average spectrum was calculated by using either Equation (1) or (2). The spectra of R_{rs} were resampled at 1 nm for further analysis. A synthetic dataset was also created by resampling Rrs measurements matching Hyperion and CHRIS bandwidths using a Gaussian function as the spectral response functions of both sensors.

2.3. Limnological Parameters

2.3.1. Chlorophyll-*a*

For the Brazilian dataset, water samples were collected from the subsurface, approximately 10 cm below the water surface, and were kept at cool temperatures until delivery to the laboratory for analysis with the duplicates. The method of chl-*a* analysis consisted of filtering the collected samples using GF/F filters (Whatman, 0.7 μm pore size) and then extracting the samples from the filters using 90% acetone and measuring the absorbance in a Varian Cary 50 Conc UV-VIS spectrophotometer (Agilent Technologies, Santa Clara, CA, USA) [24]. Concentration of chl-*a* from the spectrophotometric absorbance data was calculated using the equation from Lorenzen [25].

For the North American ponds, the chl-*a* concentrations were analyzed from the water samples collected in 1 L Niskin bottles and immediately filtered onto GF/F filters (Whatman, 0.7 μm pore size) under low vacuum (<12.7 cm of Mercury). Samples were extracted in triplicates using acetone extraction procedure and concentrations were measured using HPLC following the Environmental Protection Agency (EPA) method 447 [26].

2.3.2. Phycocyanin

During the Brazilian field campaign in April 2013, an *in situ* fluorometer called FluoroProbe (bbe Moldeanke, GmbH), was used to measure temperature and phytoplankton concentrations. The FluoroProbe data was used to distinguish phytoplankton into four groups: (1) Chlorophyta, (2) PC-rich Cyanobacteria, (3) Diatoms, and (4) Cryptophyta. All data were time stamped and archived on a field handheld personal computer. To measure PC concentration, we used a fluorometer (Turner Designs, model 10-AU-005) with a PC optical kit which uses the excitation and emission wavelengths at 600 nm and 640 nm, respectively.

During catfish pond field campaigns, water samples were filtered immediately after collection through 0.2 μm nucleopore membrane filters (Millipore) under low vacuum. The filters were stored in a 15 mL falcon tube frozen at −80 °C until analysis at the laboratory. For the analysis, filters were transferred to 50 ml polycarbonate centrifuge tubes in order to reach ambient room temperature, and then suspended in 5 mL of 50 mM phosphate buffer. Samples were homogenized using a sonicator [27] and an ice-bath was used to avoid the destruction of pigments from localized heating. The tip of the

sonicator was rinsed twice with 5 mL of 50 mM phosphate buffer each time and the rinse was collected in the centrifuge tube. Samples were centrifuged at 5 °C, 27,200 g for 25 min. This process was repeated one more time using the same settings. The supernatant was collected and absorbance was measured using a Perkin Elmer lambda 850 spectrophotometer (Perkin Elmer Inc., Waltham, MA, USA). Concentration of PC was calculated using the equation from Bennett and Bogorad [28].

2.4. Model Calibration and Validation

Three sets of calibration and validations were performed including one on the Funil Reservoir's data, one on the Catfish Pond's data, and the third on a mixed dataset. As the Funil Reservoir and Catfish Pond datasets have significantly different concentration ranges (Table 1), a third dataset was created by mixing the two and then randomly dividing into two datasets, one to be used for calibration (60%) and the other for validation (40%). Models were calibrated using the hyperspectral R_{rs} and the formulas listed in Table 2. For each model and each dataset, a linear calibration curve was set between the model values and the PC concentration. We did not use the best fit functions, which were mainly non-linear functions, to avoid an out of range calibration/validation problem because the range of PC concentration in both datasets was extreme without any overlap (Table 1).

Table 2. Summary of R_{rs} based bio-optical models used in our study for predicting PC concentration.

Name	Reference	Model
DE93	Dekker [16]	$PC \propto \left[\left(R_{rs}(600) + R_{rs}(648)\right) - R_{rs}(624)\right]$
SC00	Schalles & Yacobi [17]	$PC \propto R_{rs}(650)/R_{rs}(625)$
SI05	Simis *et al.* [10]*	$PC \propto R_{rs}(709)/R_{rs}(620)$
MI09	Mishra *et al.* [5]	$PC \propto R_{rs}(700)/R_{rs}(600)$
SM12	Mishra [29]	$PC \propto R_{rs}(709)/R_{rs}(600)$
MM09	Modified Mishra *et al.* [5]**	$PC \propto R_{rs}(724)/R_{rs}(600)$
HU10	Hunter *et al.* [11]	$PC \propto \left[\left(R_{rs}^{-1}(615) - R_{rs}^{-1}(600)\right) \cdot R_{rs}(725)\right]$

Notes: * Ratio has been adopted from Simis *et al.* [10] in their nested semi-analytical algorithm. ** MM09 is the slightly modified version of MM09.

A cross-validation procedure was adopted, if any, by developing linear calibration using one dataset and validating with the two remaining datasets (Table 3). Validations were analyzed by plotting PC Measured *versus* PC Predicted.

Table 3. Summary of calibration and validation datasets used in the study.

Calibration	Validation
Mixed dataset (n = 23)	Catfish Ponds
	Funil Reservoir
	Mixed dataset (n = 16)
Funil Reservoir	Catfish Ponds
	Mixed dataset (n = 16)
Catfish Ponds	Funil Reservoir
	Mixed dataset (n = 16)

2.5. Error Analysis

Error analysis was performed by comparing measured and predicted PC concentrations. Bias, Mean Square Error (MSE), Mean Absolute Error (MAE), and Root Mean Square Error (RMSE) were used to evaluate model performance and were calculated according to Table 4.

Table 4. Summary of error estimators used in our study.

Estimator	Formulas
Bias	$Bias = \dfrac{1}{n}\sum_{i=1}^{n}(y_i - x_i)$
MAE	$MAE = \dfrac{1}{n}\sum_{i=1}^{n}|y_i - x_i|$
MSE	$MSE = \dfrac{1}{n}\sum_{i=1}^{n}(y_i - x_i)^2$
RMSE	$RMSE = \sqrt{MSE}$

Note: where y_i and x_i are the measured and predicted PC concentration in ith sample.

2.6. Sensitivity Analysis

Sensitivity analysis was carried out for the models with the lowest errors and the best validation plots for the simulated data representing the hyperspectral satellite sensors. This analysis was performed to study chl-*a* interference on the aforementioned PC detection algorithms. The sensitivity analysis was realized using the values derived from PC detection algorithms (Table 2), chl-*a*, and PC concentrations. Surface plots were generated using these three parameters. They were analyzed according to the slope in each axes and the color scale of the surface which represents the PC detection algorithms.

3. Results and Discussion

3.1. Reflectance Characteristics

The major spectral characteristic features of pigments such as chl-*a* and PC can be noticed in the R_{rs} spectra of Funil Reservoir and catfish ponds (Figure 1). The green peak in water spectra at approximately 550 nm is commonly due to the scattering from algal cells and relatively low absorption by chl-*a* [30]. However, in our datasets the green peak is slightly displaced for the two sites, at 560 nm for catfish ponds and at 570 nm for the Brazilian reservoir, due to the difference in chl-*a* concentration range at each site. In aquatic systems with very high chl-*a* concentrations such as the catfish ponds, the spectra tend to be similar to the spectral response of vegetation. The spectral troughs near 620–625 nm and 670–675 nm appear because of strong absorption by PC and chl-*a*, respectively [17,31]. The peak at 643–650 nm appears because of the prominent absorption on both sides at 624 nm and 670 nm and also because of the phycocyanin fluorescence maximum of around 640–660 nm [17]. The main difference in the spectral shape between the two study sites occurred at the peak near 700 nm, which appears due to the strong absorption on either side, by chl-*a* at 670 nm and by water at 740 nm [5].

However, the magnitudes of the R_{rs} at 700 nm in the catfish ponds data are significantly higher than that that of Funil Reservoir because of the difference in chl-*a* concentration (Table 1).

Figure 1. R_{rs} spectra acquired from Mississippi's Catfish Ponds (red) and Funil Reservoir (blue).
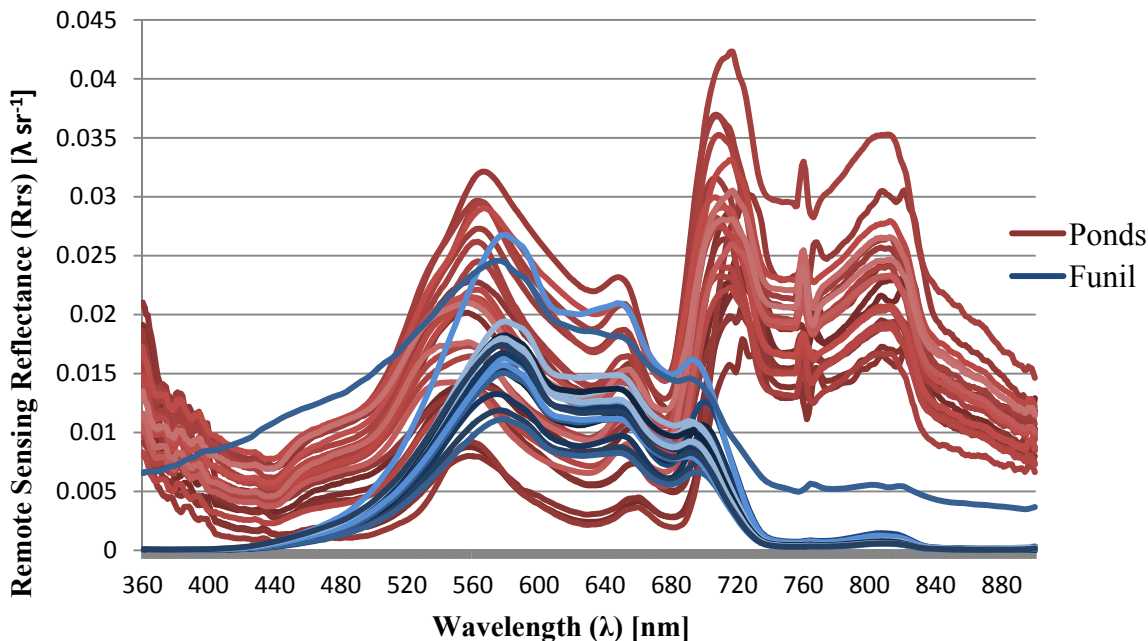
As shown in Table 1, chl-*a* concentration in Funil Reservoir varied within 4.92–52.78 μg/L, while in the catfish ponds, it was between 59.79 and 1,376.57 μg/L. PC:chl-*a* ratio varied from 0.44 to 1.90 (average = 0.91) in Funil site and between 0.30 and 3.28 (average = 1.22) in the catfish ponds. Strong dependency was found between chl-*a* and PC concentration in both datasets with R^2 of 0.89 and 0.84 for Funil Reservoir and catfish ponds, respectively (Figure 2). It corroborates with the fact that the algal community was mostly dominated by cyanobacterial biomass. Species identification was performed using microscopy and the results showed that the most abundant cyanobacteria species at the Funil Reservoir study site was *Microcystis aeruginosa* and *Planktothrix agardhii* for the catfish ponds. *Microcystis aeruginosa* is one of the most common species of cyanobacteria worldwide [31].

Figure 2. Correlation between chl-*a* and PC concentrations in both study sites.
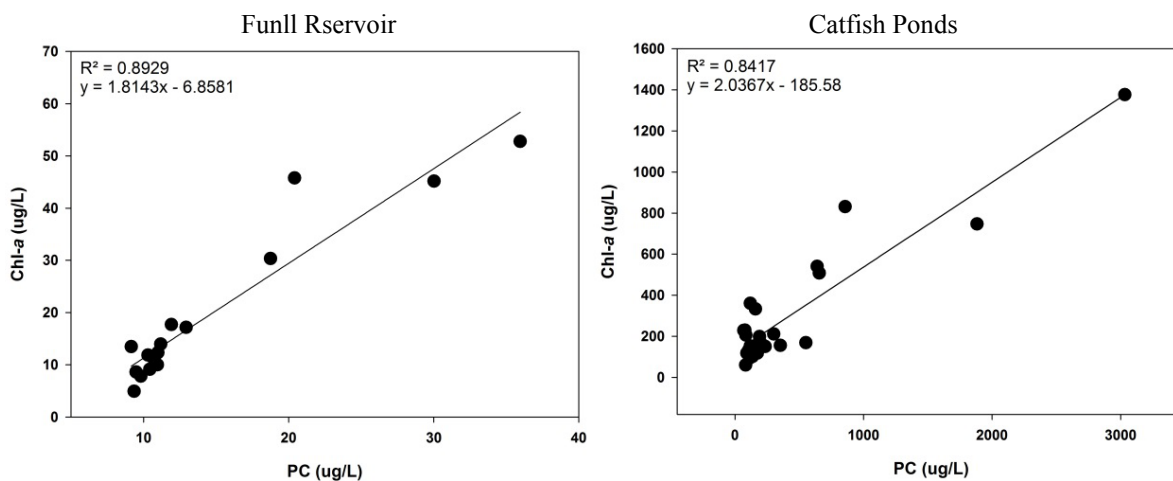
3.2. Bio-Optical Models

To analyze the relationship between PC concentrations and several bio-optical models (see Table 2), we used three datasets to calibrate the models. We used a modification of MI09 proposed by Mishra [29] referred to as SM12. SM12 targeted PC absorption at 600 nm and used the reflectance peak at 709nm. We also proposed a modification of MI09 using the reflectance peak at 724 nm which is referred to as MM09. All seven models were calibrated using a linear trend between model values and measured PC concentrations. Funil dataset calibration showed the best result with SM12 ($R^2 = 0.909$). For catfish ponds dataset, the best R^2 was found with SI05 ($R^2 = 0.748$). The mixed dataset showed the lowest R^2 among all during model calibrations and its best result was found with SI05 ($R^2 = 0.684$) (Table 5). These models presented similar results for the Adjusted R^2 confirming consistency in their performance. Calibration analysis also showed the slope (X1) and p-value for each model. DE93 and SC00 showed the highest values for slope in all the datasets. Although HU10 showed low values for its slope in the three datasets, it showed high p-values for Funil (0.179) and Catfish ponds (0.261) datasets. One of the reasons behind the poor calibration results observed for DE93 and HU10 could be the specular reflection from water under wavy conditions that generally gets suppressed in a band ratio algorithm did not get cancelled out due to the band architecture of these two algorithms [30]. The specular reflection occurs mainly due to the wind which generates waves controlling the brightness of most water pixels. Funil Reservoir is more vulnerable to wind compared to catfish ponds and the combinations of single bands used in DE93 and HU10 were not able to suppress the brightness variations due to wave disturbances. Another reason could be the choice of spectral bands used in both algorithms, since DE93 have more influence from the 648nm band which is contaminated by chl-*a* [5] and HU10 is mainly influenced by 724 nm band which is a chl-*a* reflectance peak. For accuracy assessment, models were validated by applying the linear regression equations to the other datasets (Figures 3–5). The scatter plots show the estimated PC *versus* the measured PC concentration. Although some models produced very high R^2 during the calibration with one dataset, they did not perform well on other datasets. For example, SM12 which produced the highest R^2 (0.909) during calibration, showed that it is not a good estimator for PC concentration during validation. The poor validation results could be due to the difference in the range of PC concentration at two study sites. However, the use of the mixed dataset calibration improved the validation for Funil and catfish datasets (Figures 4 and 5).

Table 5. Coefficients of determination (R^2) derived from model calibrations using the three datasets for all seven models.

Model	R^2	Adj. R^2	X1	p-value
Funil Dataset				
DE93	0.088	0.023	−664.535	0.2654
SC00	0.745	0.727	181.122	>0.0001
SI05	0.793	0.779	41.196	>0.0001
MI09	0.807	0.794	50.836	>0.0001
SM12	0.909	0.902	35.638	>0.0001
MM09	0.414	0.372	62.656	0.0072
HU10	0.125	0.062	−3.841	0.1798

Table 5. *Cont.*

Model	R^2	Adj. R^2	X1	p-value
Catfish Ponds Dataset				
DE93	0.617	0.599	1381.323	>0.0001
SC00	0.338	0.306	1622.554	0.0036
SI05	0.748	0.736	274.873	>0.0001
MI09	0.170	0.131	268.015	0.0504
SM12	0.591	0.572	344.990	>0.0001
MM09	0.731	0.718	270.868	>0.0001
HU10	0.060	0.015	−12.285	0.2611
Mixed Dataset				
DE93	0.051	0.006	5966.595	0.3016
SC00	0.518	0.495	1303.031	0.0001
SI05	0.684	0.669	132.365	>0.0001
MI09	0.547	0.525	198.107	0.0001
SM12	0.640	0.623	155.970	>0.0001
MM09	0.673	0.658	136.692	>0.0001
HU10	0.466	0.441	−13.919	0.0003

Validations for the Funil Reservoir dataset used two calibrations: the Mixed and Catfish Ponds calibrations (Figure 4). The mixed dataset calibration showed a poor accuracy for all the models tested. The catfish ponds calibrations also performed very poorly on Funil's dataset; however, HU10 produced the lowest value for the slope and showed a linear behavior. The poor performance of the bio optical models is due to the fact that linear models were chosen for the individual calibrations with Funil and catfish ponds data instead of the best-fit models, which are clearly non-linear mainly at high PC concentrations.

The use of three different datasets showing low, high and mixed ranges of PC concentrations allowed us to analyze which calibration is more accurate for different environments. For a low PC concentration environment, the calibration using HU10 and the mix dataset (wide range) produced the best validation result. For a high PC concentration environment, mix dataset calibrations also produced some of the best results with SI05 and MM09 models due to its wide range. Mixed dataset calibration also showed the best validation plots for the rest of the 40% of the mixed data using MM09.

However, if we observe the validation plots for the catfish ponds dataset in Figure 5, it is possible to notice a cloud of points in the region of low PC concentration. This cloud of points does not have a linearity which also contributes to the poor validation results. The reason for this non-linear behavior of the scatter plot could be attributed to the dominant species of cyanobacteria in the catfish ponds, the *Planktothrix agardhii.* Post *et al.* [32] described that this species can significantly increase the content of chl-*a,* thus varying the irradiance. At sampling points with low PC in the catfish ponds, the PC to chl-*a* ratio (Table 6) were also lower due to high values of chl-*a*. Thus, the high chl-*a* concentration for the points with low PC concentration, due to the specific characteristics of *Planktothrix agardhii,* could have been the reason for the cloud of points and interference in the PC estimation.

Figure 3. Validation of the models in the mixed dataset using calibrations from (1) Mixed dataset, (2) Funil Reservoir dataset, and (3) Catfish Ponds dataset.
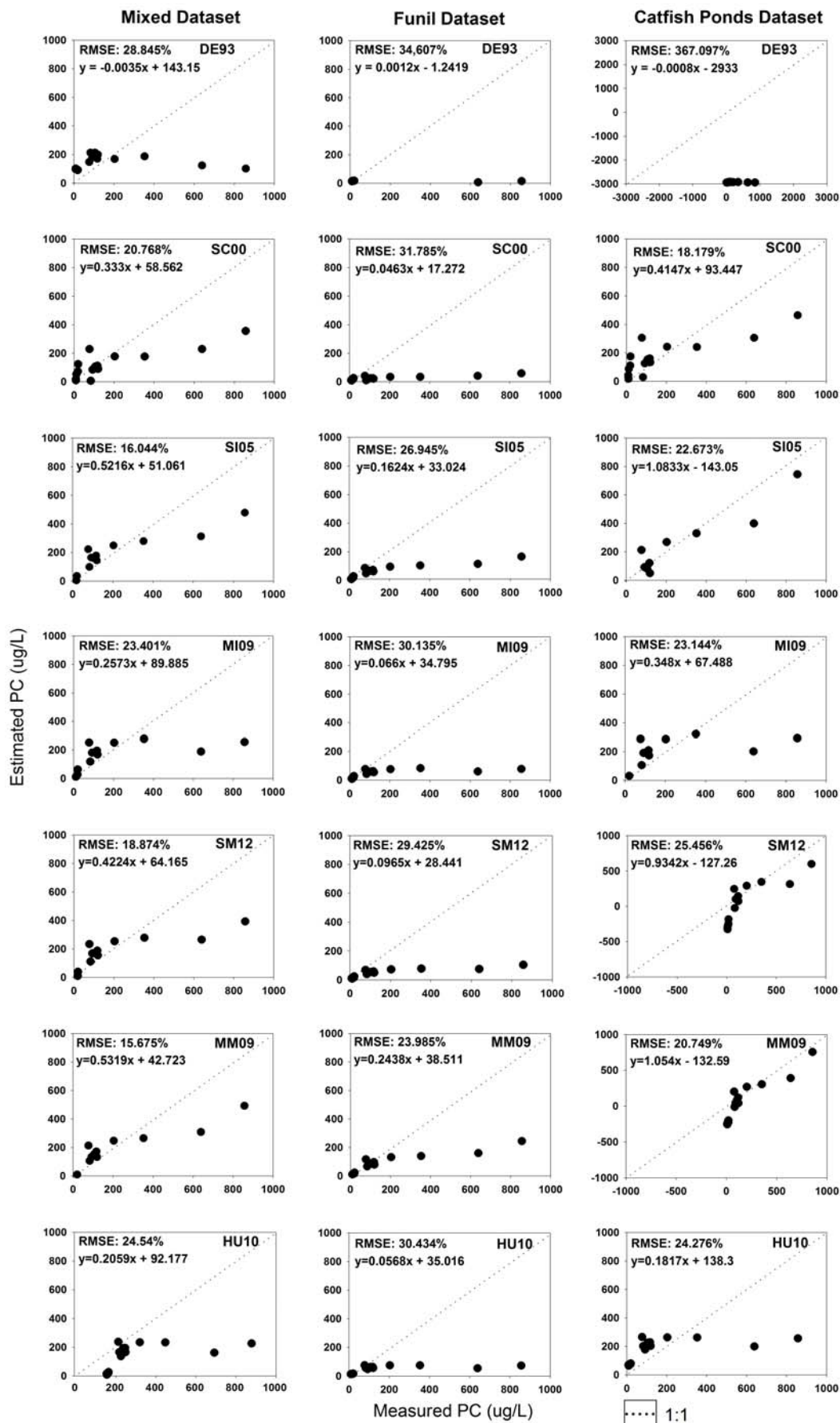
Figure 4. Validation for Funil Reservoir dataset using calibrations from (1) Mixed dataset and (3) Catfish Ponds dataset.
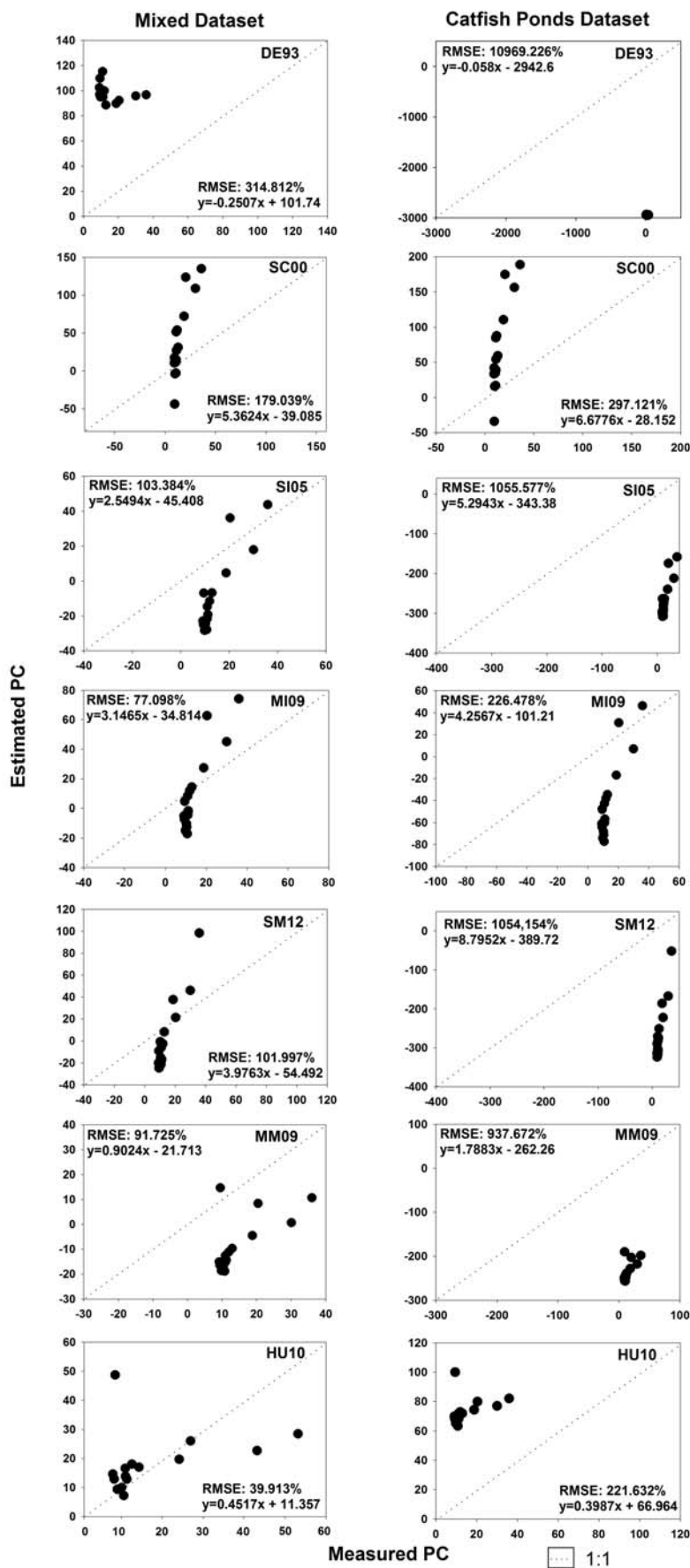
Figure 5. Validation for Catfish Pond dataset using calibrations from (1) Mixed dataset and (2) Funil Reservoir dataset.
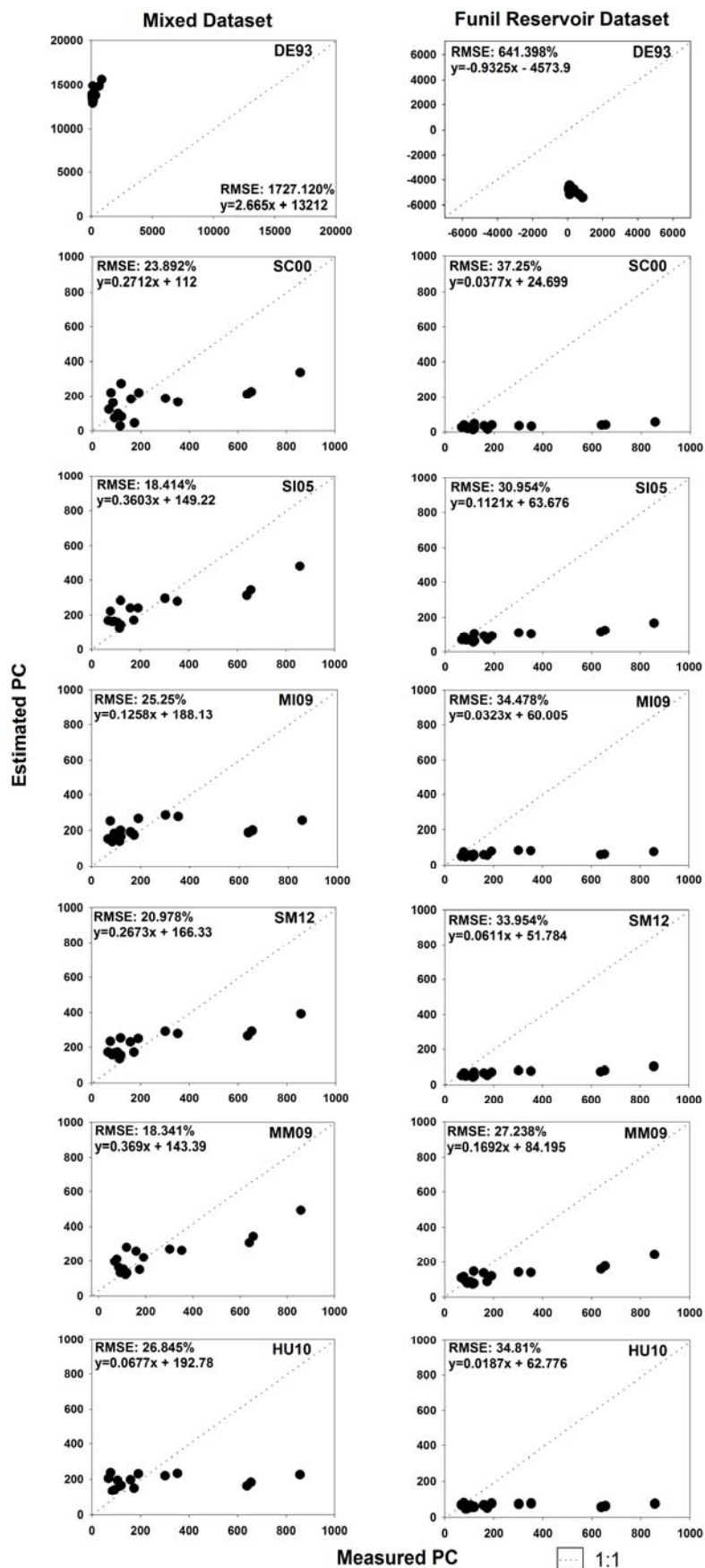
Table 6. PC and Chl-*a* ratio for the Catfish Ponds dataset.

PC	Chl-*a*	PC:Chl-*a*
68.13	228.26	0.30
77.19	229.25	0.33
83.19	59.79	1.39
84.88	205.60	0.41
92.24	117.40	0.78
105.75	131.05	0.80
114.50	94.03	1.22
116.82	109.26	1.07
118.79	360.01	0.33
119.02	152.50	0.78
119.61	130.43	0.91
136.44	101.40	1.34
159.31	332.38	0.48
173.54	117.42	1.48
191.12	198.50	0.96
203.17	164.30	1.23
234.32	149.61	1.56
301.60	210.83	1.43
352.66	155.54	2.26
550.96	168.22	3.27
639.02	539.73	1.18
655.33	507.70	1.29
857.08	831.35	1.03

Table 7 shows the error analysis for all models and for the three validation datasets. For the mixed dataset, the best results were obtained by using MM09 in the Mixed and Funil's calibrations, with an RMSE of 15.675% and 23.985%, respectively. The best catfish ponds calibration for the mixed dataset used SC00 algorithm and had a RMSE of 18.179%. The lowest errors in Funil dataset were found using HU10 model with a RMSE of 221.63% and 40.92% for catfish ponds and mixed calibrations, respectively. It showed that the errors decreased by the use of mixed calibration, enhancing the importance of using a large range of PC concentrations for the calibration of these models. These results also showed that the catfish ponds' calibration mostly overestimates the PC prediction values. On the other hand, for the catfish ponds dataset, it was observed that the models which were calibrated with low PC range perform better when compared to the opposite (predicting low PC concentration from calibrations with high PC concentration). This could be due to the fact that mostly the non-linearity or signs of saturation during calibration were observed at high PC concentrations. Overall, results showed that the MM09 was the best model for the Funil and Mixed datasets with a RMSE of 23.985% and 15.675%, respectively. These results also confirmed that it is possible to improve the accuracy of these models since the validation results (Figures 3–5) showed that there is still some residual interference at the PC absorption region. The interference was observed for data points where the PC concentration was zero but the bio-optical models produced a significant value. Interference from CDOM absorption is not an issue for the spectral range used in these models; therefore, the

residual scattering from algal pigments and TSS are the potential interference factors at these wavelengths.

Table 7. Error analysis for the linear calibrations for each model and dataset (shaded areas represent the lowest errors).

Estimator	D93	SC00	S05	M09	SM12	MM09	H10
Mixed Dataset							
Mixed Calibration							
Bias	27.884	55.119	30.472	36.709	34.287	36.062	43.176
MAE	156.034	100.247	84.726	111.710	95.558	79.642	111.087
MSE	59,821.765	31,009.467	18,507.809	39,371.406	25,612.029	17,665.301	43,296.194
RMSE	244.585	176.095	136.043	198.422	160.038	132.911	208.077
RMSE(%)	28.845	20.768	16.044	23.401	18.874	15.675	24.540
Funil Reservoir Calibration							
Bias	171.474	145.279	109.744	124.394	125.551	90.375	125.742
MAE	173.428	147.109	112.190	125.891	125.922	96.090	127.198
MSE	86,109.276	72,634.933	52,200.685	65,289.794	62,249.894	41,362.024	66,594.099
RMSE	293.444	269.509	228.475	255.519	249.499	203.377	258.058
RMSE(%)	34.607	31.785	26.945	30.135	29.425	23.985	30.434
Catfish Ponds Calibration							
Bias	3,103.557	6.313	128.852	43.635	138.474	123.386	1.175
MAE	3,103.557	105.260	154.526	125.628	174.409	147.100	140.362
MSE	9,688,859.449	23,761.486	36,958.560	38,411.144	46,590.750	30,953.637	42,369.837
RMSE	3,112.693	154.148	192.246	195.988	215.849	175.936	205.839
RMSE(%)	367.097	18.179	22.673	23.114	25.456	20.749	24.276
Funil Reservoir Dataset							
Catfish Ponds Calibration							
Bias	2,939.150	−57.184	279.993	52.170	275.038	250.650	−58.610
MAE	2,939.150	62.948	279.993	55.642	275.038	250.650	58.610
MSE	8,638,835.017	6,338.247	79,998.696	3,682.608	79,783.183	63,125.493	3,526.687
RMSE	2,939.190	79.613	282.840	60.684	282.459	251.248	59.386
RMSE(%)	10,969.226	297.121	1,055.577	226.478	1,054.154	937.672	221.632
Mixed Calibration							
Bias	−83.570	−24.276	22.903	3.636	11.262	23.130	−3.393
MAE	83.570	34.342	25.841	16.831	23.490	23.768	5.927
MSE	7,115.514	2,301.443	767.377	426.762	746.925	604.059	114.377
RMSE	84.354	47.973	27.702	20.658	27.330	24.578	10.695
RMSE(%)	314.812	179.039	103.384	77.098	101.997	91.725	39.913
Catfish Ponds Dataset							
Funil Reservoir Calibration							
Bias	5,040.604	207.704	150.849	173.707	174.972	116.461	174.222
MAE	5,040.604	207.704	151.761	173.707	174.972	126.505	174.222
MSE	25,606,599.392	86,365.614	59,637.746	73,992.014	71,760.882	46,177.712	75,424.552
RMSE	5,060.296	293.880	244.208	272.015	267.882	214.890	274.635
RMSE(%)	641.398	37.250	30.954	34.478	33.954	27.238	34.810

Table 7. *Cont.*

	Catfish Ponds Dataset						
	Mixed Calibration						
Bias	−13613.808	64.019	5.273	22.999	10.620	8.999	32.391
MAE	13613.808	128.858	104.186	128.950	115.237	104.689	140.536
MSE	185,669,971.223	35,529.975	21,105.169	39,685.667	27,393.270	20,938.331	44,856.741
RMSE	13,626.077	188.494	145.276	199.213	165.509	144.701	211.794
RMSE(%)	1727.120	23.892	18.414	25.250	20.978	18.341	26.845

3.3. Sensitivity Analysis

Sensitivity analyses were performed using the mixed dataset due to its overall strong performance and wide PC concentration range. Some of the best performing models including SC00, SI05, MI09 and MM09 were used to analyze their sensitivity to chl-*a* (Figure 6). The color scale is based on individual model outputs. Figure 6A showed that SC00 was insensitive to both chl-*a* and PC, and therefore, is not suitable to retrieve PC accurately although it was almost insensitive to chl-*a*. SI05 on the other hand showed (Figure 6B) to be a good estimator for PC concentration because of its high sensitivity to PC. However, it also showed a high sensitivity to chl-*a* (Figure 6B). In contrast, MI09 showed high sensitivity to PC and low sensitivity to chl-*a* corroborating with the fact that the chl-*a* effect on MI09 band ratio is comparatively less than other models as previously shown in Mishra *et al.* [5] (Figure 6C). MI09 was developed to avoid the residual chl-*a* absorption at the widely used PC absorption maxima, *i.e.*, at 620 nm. This was accomplished by moving the PC sensitive band to 600 nm instead of using 620 nm in the band ratio model. MM09, a modified MI09, showed high sensitivity to both PC and chl-*a* similar to SIO5 (Figure 6D).

Figure 6. Sensitivity analysis showing the interference of chl-*a* on the performance of (**A**) SC00, (**B**) SI05, (**C**) MI09, and (**D**) MM09.
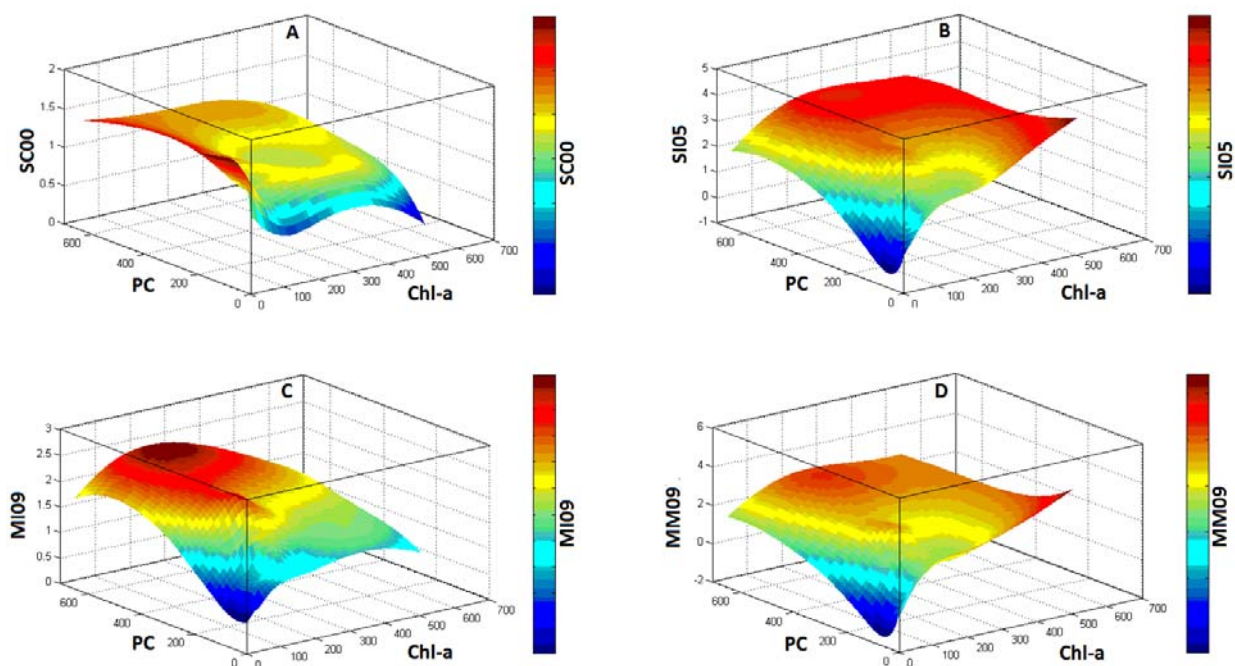
These results showed that, overall, MI09 has the least interference from chl-*a* and can be used to accurately monitor BG in widely varying water bodies. Although MI09 was developed using a dataset collected from a series of controlled laboratory experiments with two cyanobacteria species (*Synechocystis sp.* and *Anabaena sp.*) [5], our review shows that it still serves as the most accurate algorithm to be used in natural environments. To confirm the results of the sensitivity analysis, a linear regression between these models and chl-*a* concentration was conducted. The results of the regression showed that SC00 and MI09 were the models without a significant dependency on chl-*a* concentration with R^2 of 0.42 and 0.38, respectively. On the other hand to the contrary, SI05 and MM09 showed a significant dependency on chl-*a* with a R^2 of 0.65 and 0.66, respectively (results not shown). This analysis also revealed that MI09 can be used in semi-analytical algorithms to solve for PC absorption at 600 nm which can be safely assigned to PC without chl-*a* interference.

3.4. Sensor Analysis

The increasing demand for monitoring water quality in lakes and reservoirs used for water supply increases the necessity to develop accurate satellite PC products. However, most of the commonly used multispectral satellite sensors do not have the desired PC prediction band at 600 or 620 nm. The absence of specific narrow bands in multispectral sensors to target and highlight specific biophysical and biochemical parameters could be surpassed with hyperspectral sensors [33]. Reflectance products from hyperspectral satellite sensors such as Hyperion and CHRIS onboard Earth Observation 1 (EO-1), Project for On-Board Autonomy (PROBA), and the future sensor HyspIRI, which is being designed using contiguous bands with a spatial resolution of 60 m and spectral resolution of 10 nm, can be used to develop PC products and map spatial distribution of cyanobacteria in inland and coastal waters. The use of simulated HyspIRI bands for any hyperspectral models provides valuable information for next generation hyperspectral sensors from which users will have to extract appropriate optimal wavebands relevant for their application, or, as an alternative, they could carry specialized optimal sensors with selective wavebands, focusing on gathering data for targeted applications [34]. Therefore, we simulated Hyperion, CHRIS and HyspIRI spectral bands by using a Gaussian spectral response function on the field R_{rs} data [34–36]. For the Hyperion spectral bandwidth simulation, we used the bands centered at: 599.8, 609.97, 620.15, 650.67, 701.55, 711.72 and 721.9 nm. For CHRIS bandwidth simulation, we used the spectral bands centered at: 603, 613, 622, 651, 703, 709, 722 and 728 nm. For HyspIRI bandwidth simulation we used the spectral bands centered at: 605, 615, 625, 655, 705 and 725 nm. These bands were used to develop SC00, SI05, MI09 and MM09 models and used their mixed calibrations.

Results from the linear calibration/validation analysis for the Hyperion, CHRIS and HyspIRI spectral bands are presented in Table 8. Among all models, SI05 performed best by producing highest R^2 and lowest RMSE in calibration and validation for the Hyperion bands (Table 8). However, the models using CHRIS bands have a better linear calibration with a maximum R^2 of 0.72 using SI05 and lower RMSE of 14.45%. The performance of SI05 on the HyspIRI data was also better than the others with a R^2 of 0.71 and a RMSE of 14.87%.

The sensitivity analysis for Hyperion bands (Figure 7) revealed a similar behavior as shown by the hyperspectral models (Figure 6). For example, Figure 7A also shows that although SC00 was insensitive to chl-*a*, it was not a good predictor of PC concentration. MI09 showed to be most sensitive

to PC and the least sensitive to chl-*a* (Figure 7C). SI05 and MM09 performed similarly by showing sensitivity to both PC and chl-*a*. (Figure 7B, D). Overall, we noticed during sensitivity analysis that although SI05 and MM09 sometimes produced the highest R^2 and lowest RMSE during calibration and validation, their dependency on chl-*a* is consistently greater than MI09. Therefore, sometimes they also act as a strong predictor of chl-*a* concentration.

Table 8. Error analysis for linear calibrations for Hyperion and CHRIS bands.

	Hyperion		CHRIS		HyspIRI	
	R^2	RMSE (%)	R^2	RMSE (%)	R^2	RMSE (%)
SC00	0.42	23.23	0.49	16.81	0.54	18.38
SI05	0.69	15.54	0.72	14.45	0.71	14.87
MI09	0.55	22.63	0.64	18.43	0.62	20.16
MM09	0.68	16.30	0.68	15.41	0.68	15.58

Figure 7. Models using simulated Hyperion data: sensitivity analysis showing the interference of chl-*a* on the performance of (**A**) SC00, (**B**) SI05, (**C**) MI09, and (**D**) MM09.
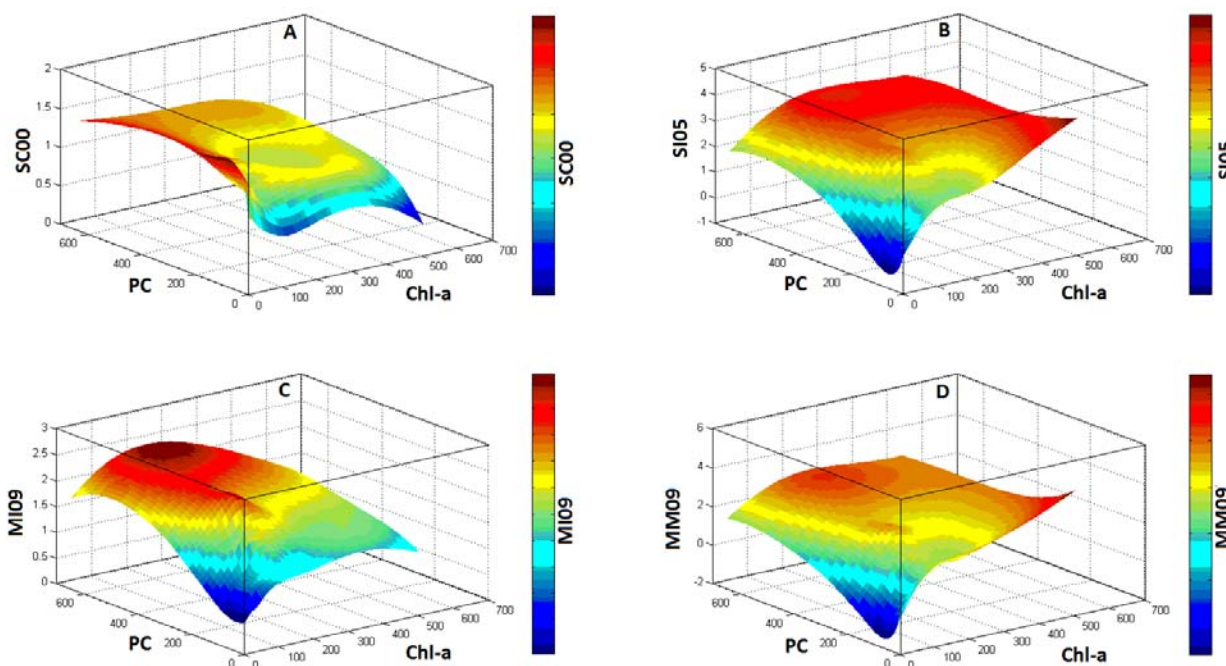
The difference in performance of Hyperion and CHRIS sensors could be attributed to the variable bandwidth of these sensors. Although data for both sensors were simulated using the Gaussian response function, the bandwidths were different. Hyperion bandwidths vary from 10.5 to 10.69 nm while CHRIS bandwidths vary from 6 to 12 nm. CHRIS has wider bandwidths near the PC absorption maxima and narrower bandwidths near the chl-*a* reflectance peak, while Hyperion bands have almost the same width in those areas. This difference can explain the models sensitivity to chl-*a* concentration, since the narrow bands enhance the spectral response in the chl-*a* reflectance peak.

The sensitivity analysis for CHRIS dataset (Figure 8) revealed that all four models are sensitive to variations in PC concentration. However, all models showed to be more sensitive to the presence of chl-*a*, having high values when the chl-*a* was also higher and low values when the chl-*a* was low.

Figure 8. Models using simulated CHRIS data: sensitivity analysis showing the interference of chl-*a* on the performance of (**A**) SC00, (**B**) SI05, (**C**) MI09, and (**D**) MM09.
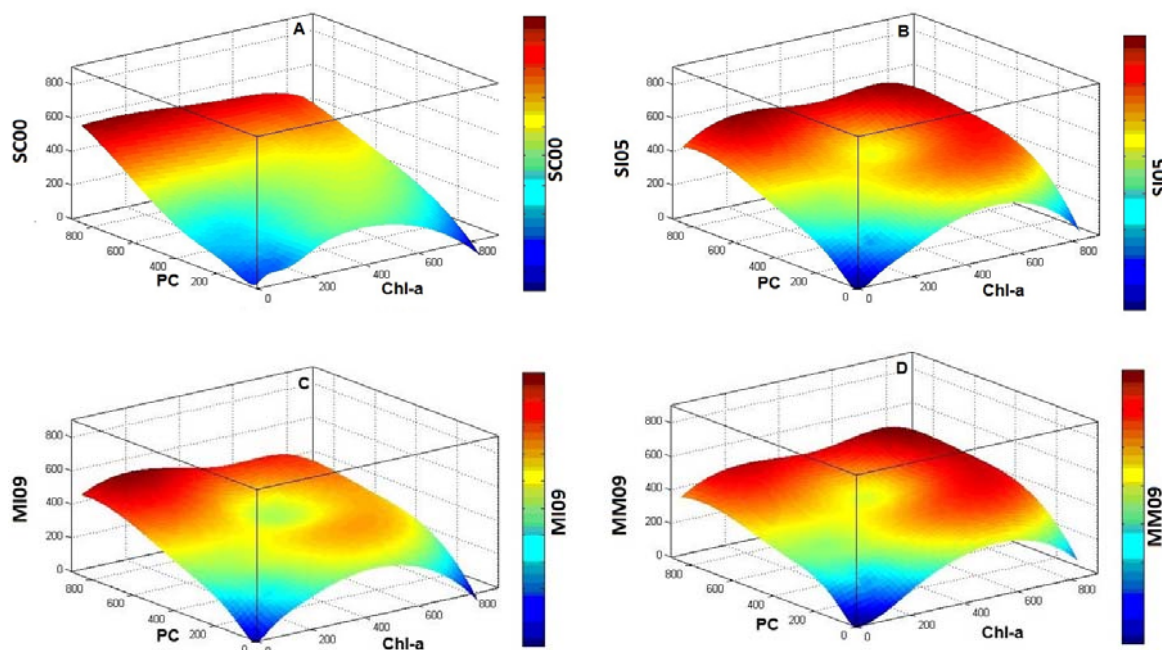
The sensitivity analysis for HyspIRI dataset (Figure 9) revealed a good sensitivity of SC00 to PC concentration. MI09 and SI05 showed a moderate sensitivity to PC concentration. However, SI05 and MM09 appeared to be more sensitive to the presence of chl-a, having high values when the chl-*a* concentration was higher and *vice versa*. On the other hand, SC00 and MI09 showed no sensitivity to chl-*a* presence. For HyspIRI, the best sensitivity performance was found in SC00, since it appeared to be sensitive to variations in PC concentration and also showed no sensitivity to chl-*a* presence

Figure 9. Models using simulated HyspIRI data: sensitivity analysis showing the interference of chl-*a* on the performance of (**A**) SC00, (**B**) SI05, (**C**) MI09, and (**D**) MM09.
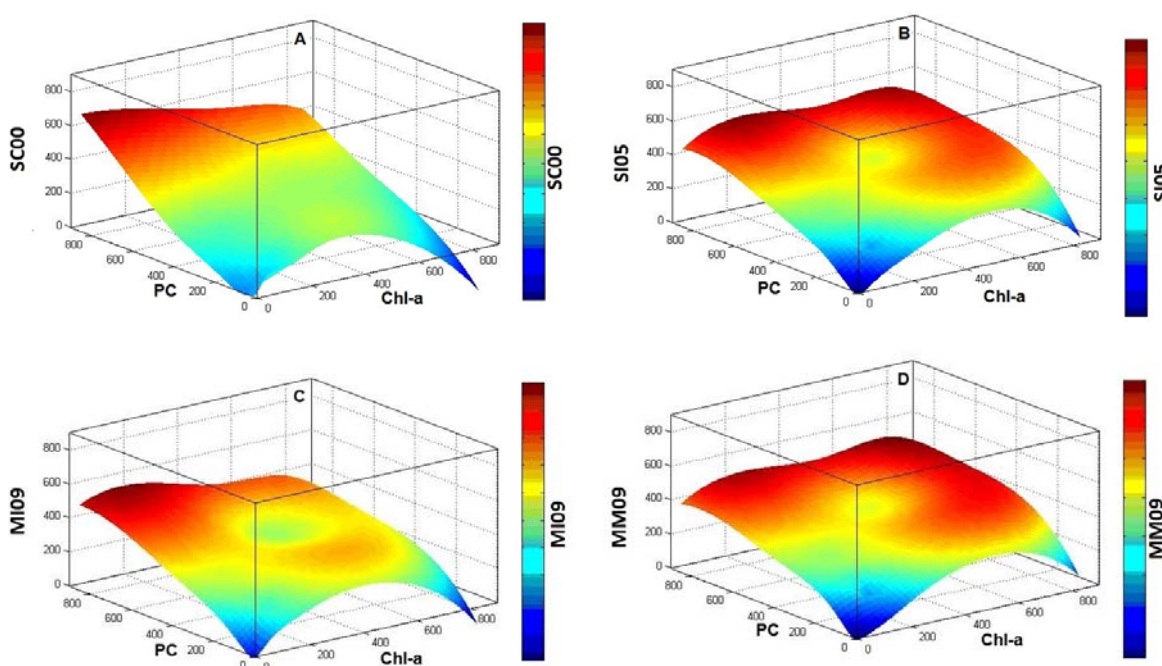
As the sensor bands confirm the algorithms input requirements, accurate atmospheric correction are required in order to avoid errors in the estimation of PC. In this research, we used proximal remote sensing measurements which do not require atmospheric correction. Therefore, applying these algorithms as described may not work for orbital sensors without an accurate atmospheric correction. However, Kutser [37] showed that the standard atmospheric correction procedures fail for water bodies with dense BG blooms since they operate under the assumption that water-leaving radiance at NIR is almost zero; but in case of a water body with dense algal bloom, that assumption is not accurate and the NIR signal cannot be ignored.

4. Conclusions

In this paper, we have reviewed and discussed the performance of all available reflectance based algorithms to predict phycocyanin (PC) content in waters with wide ranges of pigment concentration. All PC algorithms analyzed in this paper used different wavelength regions in the reflectance spectra including an absorption peak of around 600–620 nm, a fluorescence peak of around 650 nm, and a chl-*a* reflectance peak between 700 and 724 nm. We applied seven reflectance based bio-optical algorithms including Dekker [16], Schalles & Yacobi [17], Simis *et al.* [10], Mishra *et al.* [5], Mishra [29], Modified Mishra *et al.* [5], and Hunter *et al.* [11] (Table 2) for calibration and validation using three datasets that contained observations from two study sites (Catfish Ponds, MS, USA and Funil Reservoir, RJ, Brazil). Overall, we conclude that the use of chl-*a* reflectance peak near 700 nm and PC absorption at 600 nm is the best combination to be used in a PC prediction algorithm The Dekker [16] algorithm showed the highest RMSE for all the datasets. Its best performance occurred in the mixed dataset (RMSE of 28.845%) where it showed a linear relationship at low PC concentrations, however, at very high PC concentration, this relationship was no longer linear. The relatively high errors produced by the Dekker [16] algorithm in the three datasets suggest that an empirical parameterization in the calibration dataset could improve its performance. The Schalles & Yacobi [17] algorithm showed its best performance in the high PC concentrations datasets, probably because it was developed using optical data obtained in eutrophic, cyanobacteria-dominated lakes [17].

However, the use of the 650 nm band contaminates this model with strong interference from chl-*a*, thus decreasing its PC prediction capacity. Similarly, Simis *et al.* [10] showed the lowest error values for the high PC dataset, and for the low PC dataset, it did not have the same accuracy. In our datasets, chl-*a* concentration was high for the data points with low PC (*i.e.*, PC:chl-*a* ratio was low for low PC points) and therefore, interference of chl-*a* at 620 nm for low PC points was higher and affected the accuracy of the algorithm by Simis *et al.* [10]. Mishra *et al.* [5] showed the highest accuracy among all models and the least interference from chl-*a* because of the use of a band at 600 nm, and by moving away from the PC absorption maxima at 620 nm. Its derivatives, Mishra [29] and Modified Mishra *et al.* [5], used bands at 709 and 724 nm instead of at 700 and they produced mixed results with a higher sensitivity to chl-*a* compared to Mishra *et al.* [5]. Hunter *et al.* [11] showed the lowest %RMSE for the low PC data points. However, for the high PC data points, it produced high errors due to the use of two bands (600 and 615 nm) in the PC absorption region.

Overall, the sensitivity analyses were crucial in determining the efficiency of each algorithm, since it was possible to observe the interference of chl-*a* in these algorithms. Mishra *et al.* [5] appeared to be

the most insensitive algorithm to chl-*a* concentration, which also confirmed the fact that PC absorption at 600 nm has less influence of chl-*a* absorption as compared to that at 620 nm. However, the residual errors found in Mishra *et al.* [5] could be due to the enhanced interference of another water constituent, *i.e.*, the total suspended solids (TSS). More research is needed to quantify the interference of TSS at 600 nm and isolate the errors observed in Mishra *et al.* [5].

In addition, we evaluated the performance of all the PC algorithms for two spaceborne hyperspectral sensors and the upcoming HyspIRI sensor using simulated *in situ* hyperspectral data. From the analysis, it has been concluded that the three sensors can potentially be used to quantify and map PC concentration using some of the reflectance based algorithms considered in this study. However, CHRIS bands appeared to be more sensitive to chl-*a* due to its narrow bandwidth around the chl-*a* reflectance peak. Variations in the bandwidth proved to be a determinant for the accuracy of bio-optical models. Overall, results demonstrate that reflectance based algorithms can be applied to infer PC concentrations and distributions accurately using any of the three sensors.

One of the unique factors of this review paper is the datasets used in comparing the performance of various models. The datasets represent two significantly different waters in terms of their bio-optical properties, one acquired from a tropical reservoir representing oligotrophic conditions and the other from catfish ponds representing hyper-eutrophic conditions. Performance evaluation of PC detection algorithms in a tropical reservoir has not been done previously, demonstrating the presence of a research gap for low latitude areas. For example, Matthew and Bernard [38] stressed the importance of studying lower latitudes by advising future studies to focus on water types in different low latitude geographical regions of the world, mainly where data are lacking. Therefore, inclusion of a dataset from a tropical reservoir in our analysis created a significant difference in the two datasets which allowed us to test the performance and sensitivity of the reflectance based models at very low and very high PC and chl-*a* presence. We summarize that the influence of chl-*a* absorption determines the performance of a reflectance based PC prediction model, and that interference is higher at the PC absorption maxima near 620 nm than at 600 nm. Therefore, Mishra *et al.* [5] algorithm, which uses a band near 600 nm, showed the highest overall PC prediction accuracy. We conclude that for comprehensive water quality monitoring including accurate prediction of cyanobacteria content in water, a band at 600 nm is imperative in future multispectral and hyperspectral sensors.

Conflicts of Interest

The authors declare no conflict of interest.

References

1. Sun, D.; Li, Y.; Wang, Q.; Gao, J.; Le, C.; Huang, C.; Gong, S. Hyperspectral Remote Sensing of the Pigment C-Phycocyanin in Turbid Inland Waters, Based on Optical Classification. *IEEE Trans. Geosci. Remote Sens.* **2013**, *99*, 1–14.

2. Codd, G.A.; Lindsay, J.; Young, F.M.; Morrison, L.F.; Metcalf, J.S. Harmful Cyanobacteria. In *Harmful Cyanobacteria*, 1st ed.; Huisman, J., Matthijs, H.C.P., Visser, P.M., Eds.; Springer: Dordrecht, The Netherlands, 2005; Chapter 1, pp. 1–23.

3. Sivonen, K.; Jones, G. Cyanobacterial Toxins. In *Toxic Cyanobacteria in Water: A Guide to Their Public Health Consequences, Monitoring and Management*, 1st ed.; Chorus, I., Bartram, J., Eds.; UNESCO/WHO/UNEP: London, UK, 1999; Chapter 3, pp. 55–124.

4. Azevedo, S.M.F.O.; Carmichael, W.W.; Jochimsen, E.M.; Rinehart, K.L.; Lau, S.; Shaw, G.R.; Eaglesham, G.K. Human intoxication by microcystins during renal dialysis treatment in Caruaru-Brazil. *Toxicology* **2002**, *181–182*, 441–446.

5. Mishra, S.; Mishra, D.R.; Schluchter, W.M. A novel algorithm for predicting phycocyanin concentrations in cyanobacteria: A proximal hyperspectral remote sensing approach. *Remote Sens.* **2009**, *1*, 758–775.

6. Reynolds, C.S. *Ecology of Phytoplankton*, 1st ed.; Cambridge University Press: Cambridge, UK, 2006; p. 535.

7. Shapiro, J. Current beliefs regarding dominance by blue-greens: the case for the importance of CO2 and pH. *Verh. Int. Ver. Limnol.* **1990**, *24*, 38–54.

8. El-Alem, A.; Chokmani, K.; Laurion, I.; El-Adlouni, S.E. Comparative analysis of four models to estimate chlorophyll-a concentration in Case-2 waters using moderate resolution imaging spectroradiometer (MODIS) imagery. *Remote Sens.* **2012**, *4*, 2373–2400.

9. Le, C.; Li, Y.; Zha, Y.; Wang, Q.; Zhang, H.; Yin, B. Remote sensing of phycocyanin pigment in highly turbid inland waters in Lake Taihu, China. *Int. J. Remote Sens.* **2011**, *32*, 8253–8269.

10. Simis, S.G.H.; Peters, S.W.M.; Gons, H.J. Remote sensing of the cyanobacterial pigment phycocyanin in turbid inland water. *Limnol. Oceanogr.* **2005**, *50*, 237–245.

11. Hunter, P.D.; Tyler, A.N.; Carvalho, L.; Codd, G.A.; Maberly, S.C. Hyperspectral remote sensing of cyanobacterial pigments as indicators for cell populations and toxins in eutrophic lakes. *Remote Sens. Environ.* **2010**, *114*, 2705–2718.

12. Mishra, S.; Mishra, D.R.; Lee, Z.; Tucker, C.S. Quantifying cyanobacterial phycocyanin concentration in turbid productive waters: A quasi-analytical approach. *Remote Sens. Environ.* **2013**, *133*, 141–151.

13. Reinart, A.; Kutser, T. Comparison of different satellite sensors in detecting cyanobacterial bloom events in the Baltic Sea. *Remote Sens. Environ.* **2006**, *102*, 74–85.

14. Hunter, P.D.; Tyler, A.N.; Gilvear, D.J.; Willby, N.J. Using remote sensing to aid the assessment of human health risks from blooms of potentially toxic cyanobacteria. *Environ. Sci. Technol.* **2009**, *43*, 2627–2633.

15. Randolph, K.; Wilson, J.; Tedesco, L.; Li, L.; Pascual, D.P.; Soyeux, E. Hyperspectral remote sensing of cyanobacteria in turbid productive water using optically active pigments, chlorophyll a and phycocyanin. *Remote Sens. Environ.* **2008**, *112*, 4009–4019.

16. Dekker, A.G. Detection of Optical Water Quality Parameters for Eutrophic Waters by High Resolution Remote Sensing. Ph.D. Thesis, Vrije Universiteit, Amsterdam, The Netherlands, 1993.

17. Schalles, J.F.; Yacobi, Y.Z. Remote detection and seasonal patterns of phycocyanin, carotenoid, and chlorophyll pigments in eutrophic waters. *Archives Hydrobiologica* **2000**, *55*, 153–168.

18. Branco, C.W.C.; Rocha, M.I.A.; Pinto, G.F.S.; Gômara, G.A.; De Filippo, R. Limnological features of Funil Reservoir (R.J., Brazil) and indicator properties of rotifers and cladocerans of the zooplankton community. *Lakes Reservoirs: Res. Manage.* **2002**, *7*, 87–92.

19. Rocha, M.I.A.; Branco, C.W.C.; Sampaio, G.F.; Gômara, G.A.; De Filippo, R. Spatial and temporal variation of limnological features, Microcystis aeruginosa and zooplankton in a eutrophic reservoir (Funil Reservoir, Rio de Janeiro). *Acta Limnol. Brasil.* **2002**, *14*, 73–86.

20. Tucker, C.S. Ecology of channel catfish culture ponds in northwest Mississippi. *Rev. Fisheries Sci.* **1996**, *4*, 1–54.

21. Mobley, C.D. Estimation of the remote-sensing reflectance from above-surface measurements. *Appl. Optics* **1999**, *38*, 7442–7455.

22. Ohde, T.; Siegel, H. Derivation of immersion factors for the hyperspectral TriOS radiance sensor. *J. Optics A: Pure Appl. Optics* **2003**, *5*, L12–L14.

23. Austin, R.W.; Halikas, G. *The Index of Refraction of Seawater*; Visibility Laboratory-Scripps Institute of Oceanography: La Jolla, CA, USA, 1976.

24. Nush, E.A. Comparison of different methods for chlorophyll and phaeopigment determination. *Arch. Hydrobiol. Beih. Ergebn. Limnol.* **1980**, *14*, 14–36.

25. Lorenzen, C.J. Determination of chlorophyll and pheo-pigments: Spectrophotometric equations. *Limnol. Oceanogr.* **1967**, *12*, 343–346.

26. Arar, E.J. Determination of Chlorophylls a and b and Identification of Other Pigments of Interest in Marine and Freshwater Algae Using High Performance Liquid Chromatography with Visible Wavelength Detection. In *USEPA Method 447–0*; US Environmental Protection Agency: Cincinnati, OH, USA, 1997.

27. Sarada, R.; Pillai, M.G.; Ravishanker, G.A. Phycocyanin from Spirulina sp: Influence of processing of biomass on phycocyanin yield, analysis of efficacy of extraction methods and stability studies on phycocyanin. *Process. Biochem.* **1999**, *34*, 795–801.

28. Bennett, A.; Bogorad, L. Complementary chromatic adaptation in a filamentous blue-green alga. *J. Cell. Biol.* **1973**, *58*, 419–435.

29. Mishra, S. Remote Sensing of Harmful Algal Bloom. Ph.D. Thesis, Mississippi State University, Mississippi State, MS, USA, 2012.

30. Vincent, R.K.; Qin, X.M.; McKay, R.M.L.; Miner, J.; Czajkowski, K.; Savino, J.; Bridgeman, T. Phycocyanin detection from LANDSAT TM data for mapping cyanobacterial blooms in Lake Erie. *Remote Sens. Environ.* **2004**, *89*, 381–392.

31. Dall'Olmo, G.; Gitelson, A.A. Effect of bio-optical parameter variability on the remote estimation of chlorophyll-a concentration in turbid productive waters: experimental results. *Appl. Optics* **2005**, *44*, 412–422.

32. Post, A.F.; Wit, R.; Mur, L.R. Interactions between temperature and light intensity on growth and photosynthesis of the cyanobacterium Oscillatoria agardhii. *J. Plankton Res.* **1985**, *7*, 487–495.

33. Gitelson, A. Non-destructive Estimation of Foliar Pigment (chlorophylls, carotenoids, and anthocyanins) Contents: Evaluating a Semi-analytical Three-band Model. In *Hyperspectral. Remote Sensing of Vegetation*; Thenkabail, P.S., Lyon, G.J., Huete, A., Eds.; CRC Press-Taylor and Francis Group: Boca Raton, FL, USA, 2011; pp. 141–166.

34. Mariotto, I.; Thenkabail, P.S.; Huete, A.; Slonecker, E.T.; Platonov, A. Hyperspectral *versus* multispectral crop-productivity modeling and type discrimination for the HyspIRI mission. *Remote Sens. Environ.* **2013**, *139*, 291–305.

35. Cutter, M.A.; Lobb, D.R.; Williams, T.L.; Renton, R.E. Integration & Testing of the Compact High-Resolution Imaging Spectrometer (CHRIS). *Proc. SPIE* **1999**; *3753*, pp.180–191.

36. Barry, P.S.; Mendenhall, J.; Jarecke, P.; Folkman, M.; Pearlman, J.; Markham, B. EO-1 Hyperion Hyperspectral Aggregation and Comparison with EO-1 Advanced Land Imager and Landsat 7 ETM+. In Proceedings of 2002 International IEEE Geoscience and Remote Sensing Symposium, Toronto, ON, Canada, 24–28 June 2002; pp. 1648–1651.

37. Kutser, T. Quantitative detection of chlorophyll in cyanobacterial blooms by satellite remote sensing. *Limnol. Oceanogr.* **2004**, *49*, 2179–2189.

38. Matthews, M.W.; Bernard, S. Similar studies should be performed in diverse inland waters representative of other geographical regions of the world where data are lacking. *Remote Sens.* **2013**, *5*, 4370–4404.